Journal of Thermophysics and Heat Transfer
Vol. 32, No. 4, October–December 2018

Boundary Element Solver for Coupled Conduction-Radiation Heat Transfer in Nonhomogeneous Media

Yaochuang Han* and Yufeng Nie†
Northwestern Polytechnical University, Xi'an, 710129 Shaanxi, People's Republic of China
and
Yijun Liu‡
University of Cincinnati, Cincinnati, Ohio 45221-0072

DOI: 10.2514/1.T5414

In the present Paper, a boundary element solver is developed for the simulation of coupled conduction-radiation heat transfer in three-dimensional nonhomogeneous participating media. First, the boundary integral equations for radiation heat transfer in nonhomogeneous participating media are formulated. By using a simple variable transformation and with the aid of the Newton iterative scheme, the boundary integral equation for the nonlinear energy equation is obtained. For this strongly coupled system, a two-level iterative scheme is developed. Then, the boundary element method is adopted to discretize the resulting coupled system of integral equations. For the nonconvex geometries, a developed element-subdivision technique is adopted to handle with the visibility factor appearing in the radiative integral equations. Numerical examples show that the present algorithm is effective and efficient.

Nomenclature

$\mathcal{B}$	=	unit sphere in three-dimensional case
b	=	radiosity
E_b	=	blackbody emissive power
G	=	incident radiation
I	=	radiation intensity, $\mathrm{W/(m^2 \cdot sr)}$
I_b	=	blackbody intensity of radiation
i	=	irradiation
k	=	thermal conductivity, $\mathrm{W/(m \cdot K)}$
$\boldsymbol{n}$	=	unit outward normal vector
q	=	radiation heat flux, $\mathrm{W/m^2}$
r	=	distance between two points, m
S	=	boundary of domain
T	=	temperature, K
V	=	computational domain
β	=	extinction coefficient, $\sigma_a + \sigma_s$, $\mathrm{m^{-1}}$
ε	=	emissivity
ρ	=	surface reflectance
σ	=	Stefan–Boltzmann constant, $5.669 \times 10^{-8}\ \mathrm{W/(m^2 \cdot K^4)}$
σ_a	=	absorption coefficient, $\mathrm{m^{-1}}$
σ_s	=	scattering coefficient, $\mathrm{m^{-1}}$
τ	=	transmissivity
ϕ	=	angle between incident direction and normal $\boldsymbol{n}$
χ	=	visibility factor
Ω	=	single scattering albedo
ω	=	unit direction vector

I. Introduction

It is an indisputable fact that coupled conduction-radiation heat transfer (CRHT) dominates the energy transport in various high-temperature industrial applications, such as combustion chambers, furnaces, the exhaust plume, and so on. In the practical engineering environment, the distribution of the properties in the media are always nonhomogeneous. However, in the last few decades, most of the research for CRHT was carried out based on the homogeneous media. As shown in the work by Li et al. [1], the spatial variation of radiative property may significantly affect the radiative transfer, and therefore a homogeneous medium is not always a proper assumption in order to obtain accurate results for the radiation transport problems in practical applications.

The boundary element method (BEM) is a well-established numerical method, which is developed based on the boundary integral equation. During the last few decades, it has received great success in analyzing a large class of problems in science and engineering, and the interest in its application is still growing. Heat radiation is one of the physical phenomena governed by an integral equation in essence. So, it is a natural idea that heat radiation is simulated by the BEM in comparison to other numerical methods. Unfortunately, the wealth of this interesting problems does not seem to be favored by scholars, probably, in part, because of the inherent disadvantages of the BEM. The application of the BEM in radiative heat transfer analysis started in the 1990s. The first monograph was published by Bialecki [2] in 1993. The BEM solver for coupled conduction-radiation problems has been discussed in [3,4]. Qatanani et al. [5] also adopted the Galerkin BEM to simulate the radiative heat energy exchange in transparent media, and some mathematical results were presented. However, in this literature, the scattering effect is neglected. The mathematical difficulty involved in scattering is substantial. Sun et al. [6] used the BEM to simulate thermal radiation problems in a gray, absorbing, emitting, and isotropic scattering medium. The Galerkin BEM was developed for the computation of thermal radiation exchange in a diffuse, gray enclosure by Li et al. [7].

The BEM is an effective technique for the linear homogeneous boundary value problem with constant coefficients. How to solve efficiently the nonlinear and nonhomogeneous problems has always been a serious challenge for the BEM. To date, the research on this topic can be divided into two types. The first type is to look for fundamental solutions for the nonlinear and nonhomogeneous problems, such as [8,9]. However, explicit fundamental solutions can only be obtained for very limited problems. The generalized fundamental solutions, which are thermal conductivity dependent, were used by Kassab and Divo [10] to achieve boundary integral equations for this class of problems. Their technique used a generalized forcing function rather than the Dirac delta function to derive the fundamental solutions. However, this technique is difficult to handle with the heat conduction equation with the heat source term.

Received 18 November 2017; revision received 14 January 2018; accepted for publication 23 February 2018; published online 27 April 2018.

*Ph.D., Department of Applied Mathematics, 1 Dongxiang Road, Chang'an District.

†Professor, Department of Applied Mathematics, 1 Dongxiang Road, Chang'an District.

‡Professor, Mechanical Engineering.

Besides, this method also suffered some queries in [11,12]. The Green function for heat conduction in an anisotropic nonhomogeneous medium, in which the conductivities vary exponentially in one fixed but arbitrary direction, was constructed in [13]. Mikhailov [14] used the specially constructed localized parametrices to obtain the a localized boundary-domain integral or integrodifferential equation for stationary heat transfer with variable coefficients. With the aid of the radial integration method and the specially constructed parametrix (Levi function), AL-Jawary and Wrobel [15] developed a boundary-only integral equation technique for nonhomogeneous heat conduction problems with variable coefficients.

Another alternative methodology was developed by using fundamental solutions for linear homogeneous problems. In [16], a novel simple boundary element technique was presented for dealing with problems of potential flow in some special nonhomogeneous media, in which the governing equations can be transformed to the Laplace, Helmholtz, or modified Helmholtz equations. Gao [17] and Yang et al. [18] adopted the Green function for Laplace's equation and the radial integral method to obtain the boundary integral solution for nonhomogeneous heat conduction problems.

To the best of our knowledge, as far as analysis of CRHT in nonhomogeneous media using the BEM is concerned, no study has been reported so far. The present Paper is therefore aimed at extending the application of the BEM to solve CRHT in three-dimensinonal (3D) complex geometries containing a nonhomogeneous medium.

The Paper is organized as follows. In Sec. II, the boundary integral equations for radiative transfer and conduction heat transfer are derived. In Sec. III, the procedure of numerical implementation is described in detail. Numerical examples are presented in Sec. IV. The results of the numerical examples suggest that the pure BEM have the ability to handle the coupled radiation-conduction problems effectively. Finally, some conclusions are presented.

II. Mathematical Formulas

Denote by $V \subset R^3$ the bounded domain with boundary S. The diffuse boundary is assumed, which means the surface of which the outgoing intensity is independent of direction. Additionally, let the media be gray; then the physical quantities are independent of the wavelength.

A. Boundary Integral Equations for Heat Radiation

The radiative intensity at $\boldsymbol{p}$ along direction ω can be written as, see Fig. 1 [19],

$$I(\boldsymbol{p},\omega) = I(\boldsymbol{r},\omega)\tau(\boldsymbol{r},\boldsymbol{p}) + \int_{L_{rp}} \mathcal{H}(\boldsymbol{r}')\tau(\boldsymbol{r}',\boldsymbol{p})\,\mathrm{d}L(\boldsymbol{r}') \qquad (1)$$

where the source term is

$$\mathcal{H}(\boldsymbol{r}') = \sigma_a(\boldsymbol{r}')I_b(\boldsymbol{r}') + \frac{\sigma_s(\boldsymbol{r}')}{4\pi}G(\boldsymbol{r}') \qquad (2)$$

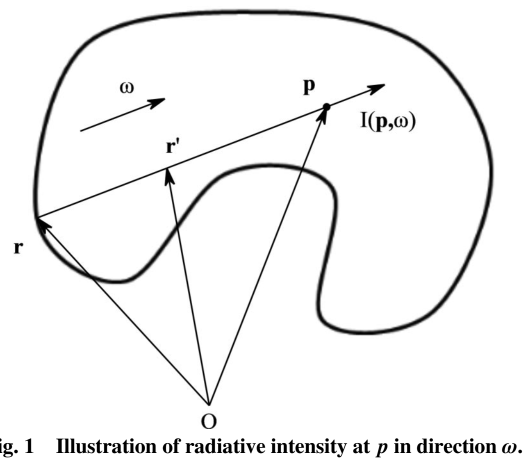

Fig. 1 Illustration of radiative intensity at *p* in direction *ω*.

$$G(\boldsymbol{r}') = \int_{\mathcal{B}} I(\boldsymbol{r}',\omega)\,\mathrm{d}(\omega) \qquad (3)$$

Let $\sigma_a(\boldsymbol{r}')$, $\sigma_s(\boldsymbol{r}')$ denote the absorption coefficient and scattering coefficient of the media at $\boldsymbol{r}'$. I_b is the blackbody intensity of radiation and is calculated by

$$I_b(\boldsymbol{r}') = \frac{1}{\pi}E_b(\boldsymbol{r}') \qquad (4)$$

where E_b denotes the blackbody emissive power and can be computed from the Stefan–Boltzmann law

$$E_b(\boldsymbol{r}') = \sigma T^4(\boldsymbol{r}') \qquad (5)$$

where σ denotes the Stefan–Boltzmann constant and $T(\boldsymbol{r}')$ is the temperature at $\boldsymbol{r}'$.

Functions $\tau(\boldsymbol{r},\boldsymbol{p})$ and $\tau(\boldsymbol{r}',\boldsymbol{p})$ in Eq. (1) are termed *transmissivities* and are defined as

$$\tau(\boldsymbol{r},\boldsymbol{p}) = \exp\left[-\int_{L_{rp}} \beta(\boldsymbol{r}')\,\mathrm{d}L(\boldsymbol{r}')\right] \qquad (6)$$

$$\tau(\boldsymbol{r}',\boldsymbol{p}) = \exp\left[-\int_{L_{r'p}} \beta(\boldsymbol{r}'')\,\mathrm{d}L(\boldsymbol{r}'')\right] \qquad (7)$$

where $\beta(\boldsymbol{r}')$ denotes the extinction coefficient of the meida at $\boldsymbol{r}'$ and $\beta = \sigma_a + \sigma_s$.

The irradiatiation for any boundary point $\boldsymbol{r}$ is defined as

$$i(\boldsymbol{r}) = \int_{n_r\cdot\omega>0} I(\boldsymbol{r},\omega)\cos\phi_r\,\mathrm{d}\omega \qquad (8)$$

where ϕ_r denotes the angle between the incident direction ω and the normal $\boldsymbol{n}_r$.

Then, the radiative heat flux at the $\boldsymbol{r}$ in direction $\boldsymbol{n}_r$ can be obtained as

$$q(\boldsymbol{r}) = \varepsilon_r i(\boldsymbol{r}) - \varepsilon_r E_b(\boldsymbol{r}) \qquad (9)$$

where ε_r denotes the emissivity at boundary point $\boldsymbol{r}$.

The radiosity at boundary point $\boldsymbol{r}$ is obtained by

$$b(\boldsymbol{r}) = \varepsilon_r E_b(\boldsymbol{r}) + \rho_r i(\boldsymbol{r}) \qquad (10)$$

where ρ_r denotes the reflexivity at $\boldsymbol{r}$ and is defined as $\rho_r = 1 - \varepsilon_r$.

Combining Eqs. (9) and (10), we have

$$b(\boldsymbol{r}) = E_b(\boldsymbol{r}) + \frac{1-\varepsilon_r}{\varepsilon_r}q(\boldsymbol{r}) \qquad (11)$$

Thanks to the diffuse boundary, the resulting intensity leaving the surface is given by [19]

$$I(\boldsymbol{r}) = b(\boldsymbol{r})/\pi \qquad (12)$$

Then, the outgoing intensity can be evaluated as

$$I(\boldsymbol{r}) = \frac{1}{\pi}\left[E_b(\boldsymbol{r}) + \frac{1-\varepsilon_r}{\varepsilon_r}q(\boldsymbol{r})\right] \qquad (13)$$

Substitute Eq. (13) into Eq. (1), and the result reads

$$I(\boldsymbol{p},\omega) = \frac{1}{\pi}\left[E_b(\boldsymbol{r}) + \frac{1-\varepsilon_r}{\varepsilon_r}q(\boldsymbol{r})\right]\tau(\boldsymbol{r},\boldsymbol{p}) + \int_{L_{rp}} \mathcal{H}(\boldsymbol{r}')\tau(\boldsymbol{r}',\boldsymbol{p})\,\mathrm{d}L(\boldsymbol{r}') \qquad (14)$$

With the aid of Eqs. (8), (9), and (14), the radiative heat flux can be obtained as follows:

$$q(\boldsymbol{p})+\varepsilon_p E_b(\boldsymbol{p})=\frac{\varepsilon_p}{\pi}\int_{n_p\cdot\omega>0}\left[E_b(\boldsymbol{r})+\frac{1-\varepsilon_r}{\varepsilon_r}q(\boldsymbol{r})\right]\tau(\boldsymbol{r},\boldsymbol{p})\cos\phi_p\,\mathrm{d}\omega$$
$$+\int_{n_p\cdot\omega>0}\left[\int_{L_{rp}}\mathcal{H}(\boldsymbol{r}')\tau(\boldsymbol{r}',\boldsymbol{p})\,\mathrm{d}L(\boldsymbol{r}')\right]\cos\phi_p\,\mathrm{d}\omega \tag{15}$$

Using the geometrical relationship [20]

$$d\omega=\frac{\cos\phi_r}{|\boldsymbol{r}-\boldsymbol{p}|^{d-1}}dS(\boldsymbol{r}) \tag{16}$$

and Eq. (2), Eq. (15) can be transformed as

$$q(\boldsymbol{p})+\varepsilon_p E_b(\boldsymbol{p})=\frac{\varepsilon_p}{\pi}\int_S\left[E_b(\boldsymbol{r})+\frac{1-\varepsilon_r}{\varepsilon_r}q(\boldsymbol{r})\right]\tau(\boldsymbol{r},\boldsymbol{p})K_1(\boldsymbol{r},\boldsymbol{p})\,\mathrm{d}S(\boldsymbol{r})$$
$$+\varepsilon_p\int_S\left[\int_{L_{rp}}\mathcal{H}(\boldsymbol{r}')\tau(\boldsymbol{r}',\boldsymbol{p})\,\mathrm{d}L(\boldsymbol{r}')\right]K_1(\boldsymbol{r},\boldsymbol{p})\,\mathrm{d}S(\boldsymbol{r}) \tag{17}$$

where

$$K_1(\boldsymbol{r},\boldsymbol{p})=\frac{\cos\phi_r\cos\phi_p}{|\boldsymbol{r}-\boldsymbol{p}|^2}\chi(\boldsymbol{r},\boldsymbol{p}) \tag{18}$$

According to Eqs. (3), (14), and (16), the incident radiation is calculated by

$$G(\boldsymbol{p})=\frac{1}{\pi}\int_S\left[E_b(\boldsymbol{r})+\frac{1-\varepsilon_r}{\varepsilon_r}q(\boldsymbol{r})\right]\tau(\boldsymbol{r},\boldsymbol{p})K_2(\boldsymbol{r},\boldsymbol{p})\,\mathrm{d}S(\boldsymbol{r})$$
$$+\int_S\left[\int_{L_{rp}}\mathcal{H}(\boldsymbol{r}')\tau(\boldsymbol{r}',\boldsymbol{p})\,\mathrm{d}L(\boldsymbol{r}')\right]K_2(\boldsymbol{r},\boldsymbol{p})\,\mathrm{d}S(\boldsymbol{r}) \tag{19}$$

where

$$K_2(\boldsymbol{r},\boldsymbol{p})=\frac{\cos\phi_r}{|\boldsymbol{r}-\boldsymbol{p}|^2}\chi(\boldsymbol{r},\boldsymbol{p}) \tag{20}$$

The visibility factor χ in kernels K_1 and K_2, named *the shadow zone function*, is defined as

$$\chi(\boldsymbol{r},\boldsymbol{p})=\begin{cases}1, & \text{if } \boldsymbol{r} \text{ can be seen by } \boldsymbol{p},\\ 0, & \text{otherwise}\end{cases}$$

Here, the statement "$\boldsymbol{r}$ can be seen by $\boldsymbol{p}$" means that there is no opaque material between $\boldsymbol{r}$ and $\boldsymbol{p}$, (i.e., $\overline{\boldsymbol{rp}}\cap S=\varnothing$).

Once the temperatures of both the medium and the bounding surface are known, Eqs. (17) and (19) constitute a closed system of equations to be solved about unknown quantities q and G. This integral system is a form of integral equations for radiative transfer in nonhomogeneous participating media with isotropic scattering.

B. Boundary Integral Equation for Heat Conduction

The steady-state energy conservation equation for conduction-radiation heat transfer in nonhomogeneous media is given by [19]

$$-\nabla\cdot[k(\boldsymbol{p})\nabla T(\boldsymbol{p})]+4\sigma_a(\boldsymbol{p})\sigma T^4(\boldsymbol{p})=\sigma_a(\boldsymbol{p})G(\boldsymbol{p}),\quad \boldsymbol{p}\in V \tag{21}$$

where $k(\boldsymbol{p})$ denotes the thermal conductivity at $\boldsymbol{p}$.

With the appropriate boundary condition,

$$T(\boldsymbol{p})=\bar{T}(\boldsymbol{p}),\quad \boldsymbol{p}\in S_1,$$
$$k(\boldsymbol{p})\frac{\partial T(\boldsymbol{p})}{\partial\boldsymbol{n}}=\bar{q}(\boldsymbol{p}),\quad \boldsymbol{p}\in S_2$$

where $\bar{S}_1\cup\bar{S}_2=S$ and $S_1\cap S_2=\varnothing$.

From the energy equation, it is obvious that the bridge linking conduction and radiation is the incident radiation G.

To simulate Eq. (21) by the BEM, a simple variable transformation technique was developed by Sutradhar and Paulino [16] in 2004. First, a new variable is defined as

$$v(\boldsymbol{p})=\sqrt{k(\boldsymbol{p})}T(\boldsymbol{p}) \tag{22}$$

Then, we have

$$\nabla^2 v(\boldsymbol{p})=\left[\frac{\nabla^2 k(\boldsymbol{p})}{2k(\boldsymbol{p})}-\frac{\nabla k(\boldsymbol{p})\cdot\nabla k(\boldsymbol{p})}{4k^2(\boldsymbol{p})}\right]\sqrt{k(\boldsymbol{p})}T(\boldsymbol{p})$$
$$+\sqrt{k(\boldsymbol{p})}\nabla\cdot[k(\boldsymbol{p})\nabla T(\boldsymbol{p})] \tag{23}$$

Substituting Eq. (21) and the transformation Eq. (22) into Eq. (23), we can obtain the following equation:

$$\nabla^2 v(\boldsymbol{p})=\left[\frac{\nabla^2 k(\boldsymbol{p})}{2k(\boldsymbol{p})}-\frac{\nabla k(\boldsymbol{p})\cdot\nabla k(\boldsymbol{p})}{4k^2(\boldsymbol{p})}\right]v(\boldsymbol{p})$$
$$+\sqrt{k(\boldsymbol{p})}\left[\frac{4\sigma_a(\boldsymbol{p})\sigma}{k^2(\boldsymbol{p})}v^4(\boldsymbol{p})-\sigma_a(\boldsymbol{p})G(\boldsymbol{p})\right],\quad \boldsymbol{p}\in V \tag{24}$$

The boundary condition of the original problem can be changed as follows:

$$v(\boldsymbol{p})=\sqrt{k(\boldsymbol{p})}\bar{T}(\boldsymbol{p}),\quad \boldsymbol{p}\in S_1,$$
$$\frac{\partial v(\boldsymbol{p})}{\partial\boldsymbol{n}}=\frac{1}{2k(\boldsymbol{p})}\frac{\partial k(\boldsymbol{p})}{\partial\boldsymbol{n}}v(\boldsymbol{p})-\frac{\bar{q}(\boldsymbol{p})}{\sqrt{k(\boldsymbol{p})}},\quad \boldsymbol{p}\in S_2$$

Equation (24) is a semilinear partial differential equation. To adopt the BEM to solve Eq. (24), an iterative scheme is necessary. Here, the Newton iterative scheme is adopted, that is,

$$-\nabla^2 v^{(n+1)}(\boldsymbol{p})$$
$$+\left\{\frac{\nabla^2 k(\boldsymbol{p})}{2k(\boldsymbol{p})}-\frac{\nabla k(\boldsymbol{p})\cdot\nabla k(\boldsymbol{p})}{4k^2(\boldsymbol{p})}+\frac{16\sigma\sigma_a(\boldsymbol{p})}{k^{3/2}(\boldsymbol{p})}[v^{(n)}(\boldsymbol{p})]^3\right\}v^{(n+1)}(\boldsymbol{p})$$
$$=\sigma_a(\boldsymbol{p})\sqrt{k(\boldsymbol{p})}\left\{\frac{12\sigma}{k^2(\boldsymbol{p})}[v^{(n)}(\boldsymbol{p})]^4+G^{(n)}(\boldsymbol{p})\right\},\quad \boldsymbol{p}\in V \tag{25}$$

where $v^{(n)}$ denotes the nth iterative solution.

Let

$$\alpha(\boldsymbol{p})=\frac{\nabla^2 k(\boldsymbol{p})}{2k(\boldsymbol{p})}-\frac{\nabla k(\boldsymbol{p})\cdot\nabla k(\boldsymbol{p})}{4k^2(\boldsymbol{p})}+\frac{16\sigma\sigma_a(\boldsymbol{p})}{k^{3/2}(\boldsymbol{p})}[v^{(n)}(\boldsymbol{p})]^3 \tag{26}$$

$$g(\boldsymbol{p})=\sigma_a(\boldsymbol{p})\sqrt{k(\boldsymbol{p})}\left\{\frac{12\sigma}{k^2(\boldsymbol{p})}[v^{(n)}(\boldsymbol{p})]^4+G^{(n)}(\boldsymbol{p})\right\} \tag{27}$$

Then, Eq. (25) can be rewritten as

$$-\nabla^2 v(\boldsymbol{p})+\alpha(\boldsymbol{p})v(\boldsymbol{p})=g(\boldsymbol{p}),\qquad \boldsymbol{p}\in V \tag{28}$$

Finally, Eq. (21) is transformed as a Helmholtz-type equation with variable coefficients, that is, Eq. (28). Suppose that $G(\boldsymbol{p},\boldsymbol{r})$ denotes the fundamental solution of Laplace's equation and $v(\boldsymbol{p})$ is the unknown function that satisfies Eq. (28). By the use of Green's second identity, the following equation is valid:

$$\int_V \nabla^2 vG - \nabla^2 Gv \, \mathrm{d}V = \int_S \frac{\partial v}{\partial \boldsymbol{n}} G - \frac{\partial G}{\partial \boldsymbol{n}} v \, \mathrm{d}S \tag{29}$$

Applying Eq. (28), we obtain

$$\int_S \frac{\partial v}{\partial \boldsymbol{n}} G - \frac{\partial G}{\partial \boldsymbol{n}} v \, \mathrm{d}S = \int_V \nabla^2 vG - \nabla^2 Gv \, \mathrm{d}V = \int_V f(\boldsymbol{p}) G(\boldsymbol{p}, \boldsymbol{r}) \, \mathrm{d}V(\boldsymbol{p}) + \frac{\alpha(\boldsymbol{r})}{2\pi} v(\boldsymbol{r}) \tag{30}$$

where $\alpha(\boldsymbol{r})$ is the internal angle with regard to the collocation point, and

$$f(\boldsymbol{p}) = g(\boldsymbol{p}) - \alpha(\boldsymbol{p}) v(\boldsymbol{p}) \tag{31}$$

How to solve the domain integral in Eq. (30) may be the remaining main issue here. In this Paper, we adopt the technique of subtraction of singularity, that is,

$$\int_V f(\boldsymbol{p}) G(\boldsymbol{p}, \boldsymbol{r}) \, \mathrm{d}V(\boldsymbol{p}) = \int_V (f(\boldsymbol{p}) - f(\boldsymbol{r})) G(\boldsymbol{p}, \boldsymbol{r}) \, \mathrm{d}V(\boldsymbol{p}) + f(\boldsymbol{r}) \int_V G(\boldsymbol{p}, \boldsymbol{r}) \, \mathrm{d}V(\boldsymbol{p}) = I_V^1(\boldsymbol{r}) + f(\boldsymbol{r}) I_V^2(\boldsymbol{r}) \tag{32}$$

Because of the weak singularity in G, we have

$$\lim_{r \to p} [f(\boldsymbol{p}) - f(\boldsymbol{r})] G(\boldsymbol{p}, \boldsymbol{r}) = 0 \tag{33}$$

So, I_V^1 can be calculated easily with no singularity by the use of the local numerical scheme.

If there exists a function $G^*(\boldsymbol{p}, \boldsymbol{r})$, which satisfies

$$\nabla^2 G^* = G \tag{34}$$

then Eq. (34) can be solved as

$$G^*(\boldsymbol{p}, \boldsymbol{r}) = \frac{1}{8\pi} r \tag{35}$$

where r is the distance between $\boldsymbol{p}$ and $\boldsymbol{r}$.

Substituting Eq. (34) into I_V^2 and applying the divergence theorem, then we have

$$I_V^2(\boldsymbol{r}) = f(\boldsymbol{r}) \int_V \nabla^2 G^*(\boldsymbol{p}, \boldsymbol{r}) \, \mathrm{d}V(\boldsymbol{p}) = f(\boldsymbol{r}) \int_S \frac{\partial G^*(\boldsymbol{p}, \boldsymbol{r})}{\partial \boldsymbol{n}} \, \mathrm{d}S(\boldsymbol{p}) \tag{36}$$

Then, we can obtain the boundary-domain integral equation for Eq. (28) as

$$\frac{\alpha(\boldsymbol{r})}{2\pi} v(\boldsymbol{r}) = \int_S \frac{\partial v}{\partial \boldsymbol{n}} G \, \mathrm{d}S - \int_S \frac{\partial G}{\partial \boldsymbol{n}} v \, \mathrm{d}S - \int_V [f(\boldsymbol{p}) - f(\boldsymbol{r})] G(\boldsymbol{p}, \boldsymbol{r}) \, \mathrm{d}V - f(\boldsymbol{r}) \int_S \frac{\partial G^*}{\partial \boldsymbol{n}} \, \mathrm{d}S \tag{37}$$

C. Discretization and Numerical Implementation

In this Paper, we adopt the constant element to discretize the boundary. That is, the boundary is approximated by N plane boundary elements $\{S_i\}_{i=1}^N$. The discrete points $\boldsymbol{r}_i$ are collocated at the center of S_i for $i = 1, \ldots, N$. The boundary values are approximated constantly over the boundary elements. To deal with the line integral in Eqs. (17) and (19) and the domain integral in Eq. (37), the whole domain is covered by a set of cuboid cells. The temperature field and the incident radiation are approximated constantly over these regular cells, and the interior collocation points are located on the center of the cells.

Based on the previous discretization, Eqs. (17) and (19) can be approximated as

$$q(\boldsymbol{p}_i) + \varepsilon_{p_i} E_b(\boldsymbol{p}_i) = \frac{\varepsilon_{p_i}}{\pi} \sum_{j=1}^N \left[E_b(\boldsymbol{r}_j) + \frac{1 - \varepsilon_{r_j}}{\varepsilon_{r_j}} q(\boldsymbol{r}_j) \right] \int_{S_j} \tau(\boldsymbol{r}, \boldsymbol{p}) K_1(\boldsymbol{r}, \boldsymbol{p}) \, \mathrm{d}S(\boldsymbol{r}) + \varepsilon_{p_i} \sum_{j=1}^N \int_{S_j} \left[\sum_{k=1}^L \mathcal{H}(\boldsymbol{r}_k') \int_{L_{rp_i}^k} \tau(\boldsymbol{r}', \boldsymbol{p}) \, \mathrm{d}L_{rp}(\boldsymbol{r}') \right] K_1(\boldsymbol{r}, \boldsymbol{p}) \, \mathrm{d}S(\boldsymbol{r}) \tag{38}$$

where $\boldsymbol{p}_i$ is given (in turn) by all the boundary collocation points,

$$G(\boldsymbol{p}_i) = \frac{1}{\pi} \sum_{j=1}^N \left[E_b(\boldsymbol{r}_j) + \frac{1 - \varepsilon_{r_j}}{\varepsilon_{r_j}} q(\boldsymbol{r}_j) \right] \int_{S_j} \tau(\boldsymbol{r}, \boldsymbol{p}) K_2(\boldsymbol{r}, \boldsymbol{p}) \, \mathrm{d}S(\boldsymbol{r}) + \sum_{j=1}^N \int_{S_j} \left[\sum_{k=1}^L \mathcal{H}(\boldsymbol{r}_k') \int_{L_{rp_i}^k} \tau(\boldsymbol{r}', \boldsymbol{p}) \, \mathrm{d}L_{rp}(\boldsymbol{r}') \right] K_2(\boldsymbol{r}, \boldsymbol{p}) \, \mathrm{d}S(\boldsymbol{r}) \tag{39}$$

where $\boldsymbol{p}_i$ is given (in turn) by all the interior collocation points.

The main issue for the simulation of Eqs. (17) and (19) is how to deal with the visibility factor χ, as is shown in the kernels K_1 and K_2. In this Paper, a high-precision detecting algorithm developed in [21] is adopted. By using this algorithm, the shadow zones can be captured accurately.

Remark 1: The detecting algorithm in [21] adopts element refinement strategy. The subdivision is terminated when the area of the produced subelement reaches a preset minimum value. Theoretically, this algorithm can capture the shadow zone exactly when the preset minimum value approximates zero.

The domain integral I_V^1 in Eq. (37) can be approximated as

$$I_V^1(\boldsymbol{r}) \simeq \sum_{j=1}^M [f(\boldsymbol{p}_j) - f(\boldsymbol{r})] G(\boldsymbol{p}_j, \boldsymbol{r}) S_j \tag{40}$$

where $S_j = \int_{V_j} \mathrm{d}V$, and $\boldsymbol{p}_j$ denotes the interior collocation point located in cell V_j.

Then, the discrete version of Eq. (31) can be expressed as

$$\frac{\alpha(\boldsymbol{r}_i)}{2\pi} v(\boldsymbol{r}_i) = \sum_{j=1}^N q(\boldsymbol{r}_j) \int_{S_j} G(\boldsymbol{r}_j, \boldsymbol{r}) \mathrm{d}S(\boldsymbol{r}) - \sum_{j=1}^N v(\boldsymbol{r}_j) \int_{S_j} \frac{\partial G(\boldsymbol{r}_j, \boldsymbol{r})}{\partial \boldsymbol{n}} \mathrm{d}S(\boldsymbol{r}) + \sum_{k=1}^M [f(\boldsymbol{p}_k) - f(\boldsymbol{r}_i)] G(\boldsymbol{p}_k, \boldsymbol{r}_i) S_k + \sum_{j=1}^N \int_{S_j} \frac{\partial G^*(\boldsymbol{r}_j, \boldsymbol{r})}{\partial \boldsymbol{n}} \mathrm{d}S \tag{41}$$

where $\boldsymbol{r}_i$ is given (in turn) by all the boundary and interior collocation points.

When constant elements are used, all the singular integrals in Eq. (41) can be evaluated analytically (see the Appendix).

After applying the corresponding boundary condition to Eq. (41), we can obtain the discretization system

$$\boldsymbol{A}\boldsymbol{x} = \boldsymbol{b} \tag{42}$$

which should be solved to obtain the unknown entries of v on the boundary and in the interior and $\partial v / \partial \boldsymbol{n}$ on the boundary.

Because of the strong coupling nature, the coupled conduction-radiation heat transfer system would better be solved by adopting the iterative technique. Additionally, because the resulting discrete system of Eqs. (17) and (19) is typically a large size, direct solution methods are impractical. Another iterative method is suggested to solve Eqs. (17) and (19). Then, the two-level iterative mode is adopted to simulate this coupled heat transfer system. Given an initial temperature field and incident radiation field, Eqs. (17) and (19) are solved iteratively. Using the convergent incident radiation, the energy equation is solved to update the temperature field. Repeat this procedure until the difference between the temperature field of the two iterations is less than a preset tolerance. A detailed flow diagram of the present algorithm is shown in Fig. 2.

III. Numerical Examples

A. Example 1

A classical unit cube enclosing an isothermal, absorbing, emitting, and isotropically scattering medium is considered. All the surfaces of the enclosure are cold and black, so there is no emission or reflection from the boundaries. Radiative properties in the medium are influenced by a shaped optical thickness for which the extinction coefficient varies according to the relation

$$\beta(x,y,z) = 0.9(1\text{–}2|x|)(1\text{–}2|y|)(1\text{–}2|z|) + 0.1\ (\mathrm{m}^{-1})$$

where the coordinate orgin lies at the cube center.

In this example, the boundary of enclosure is discretized with 486 boundary square elements. The inner of the geometry is covered by a $9\times9\times9$ orthogonal mesh of cubic subvolumes. The results of dimensionless radiative heat flux are represented and compared with existing results in Tables 1 and 2 [22–24].

Table 1 Surface heat fluxes at $(-0.5, 0, z)$

	$\Omega = 0$				
z	Monte Carlo method [22]	Discrete transfer method [22]	YIX [23]	Finite element method [24]	BEM
$\pm4/9$	0.10857	0.10967	0.10872	0.10743	0.10358
$\pm3/9$	0.14012	0.14107	0.14171	0.13759	0.13558
$\pm2/9$	0.16566	0.16645	0.16619	0.16255	0.16116
$\pm1/9$	0.18468	0.18543	0.18552	0.18049	0.17977
0	0.19239	0.19286	0.19260	0.18760	0.18696

Table 2 Surface heat fluxes at $(-0.5, 0, z)$

	$\Omega = 0.9$				
z	Monte Carlo method [22]	Discrete transfer method [22]	YIX [23]	Finite element method [24]	BEM
$\pm4/9$	0.01213	0.01217	0.01214	0.01193	0.01156
$\pm3/9$	0.01573	0.01574	0.01589	0.01536	0.01519
$\pm2/9$	0.01867	0.01870	0.01877	0.01826	0.01818
$\pm1/9$	0.02104	0.02094	0.02107	0.02037	0.02038
0	0.02182	0.02182	0.02192	0.02120	0.02123

B. Example 2

This test case deals with the 3D L-shaped enclosure (Fig. 3), which was previously investigated by [22,25]. All the walls are cold and black with an emissive power equal to 0.25. An isothermal, absorbing, emitting, and isotropically scattering medium, with unity blackbody emissive power, is assumed. The extinction coefficient varies according to the expressions

$$x \le -y:\ \beta(x,y,z) = 0.9(1.5+x)(1\text{–}2|y|)(1\text{–}2|z|)/(1.5-y) + 0.1\ (\mathrm{m}^{-1}),$$

$$x > -y:\ \beta(x,y,z) = 0.9(1\text{–}2|x|)(2.5-y)(1\text{–}2|z|)/(2.5+x) + 0.1\ (\mathrm{m}^{-1})$$

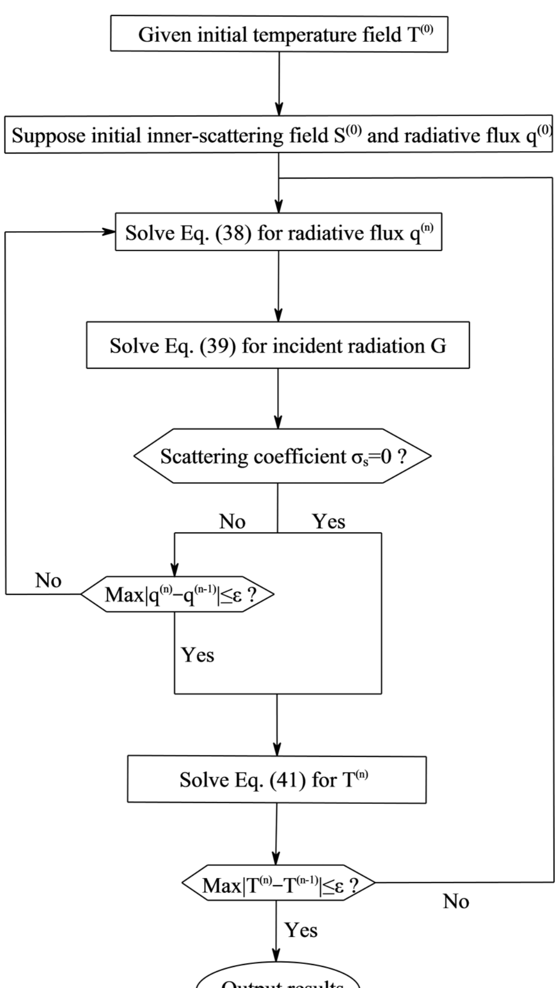

Fig. 2 The algorithm flow.

In simulation, the boundary of enclosure is discretized with 882 boundary linear elements. The inner part of the geometry is covered by a $14\times20\times7$ orthogonal mesh of cubic subvolumes. The results of dimensionless radiative heat flux along the two lines AA and BB, as shown in Fig. 3, are represented and compared with existing results in Fig. 4.

C. Example 3

Radiative heat transfer in cylindrical media is important in various industrial applications. So, the cylindrical geometry, as is shown in Fig. 5, is considered in this example. The parameters are presented in Table 3, in which $r = \sqrt{(x^2+y^2)}$ and ϵ_1, ϵ_2, and ϵ_3 denote the emissivity of the bottom surface, top surface, and side surface, respectively. The current results are compared with previous results [26,27] in Fig. 6. The results in [26,27] are obtained by calculating the

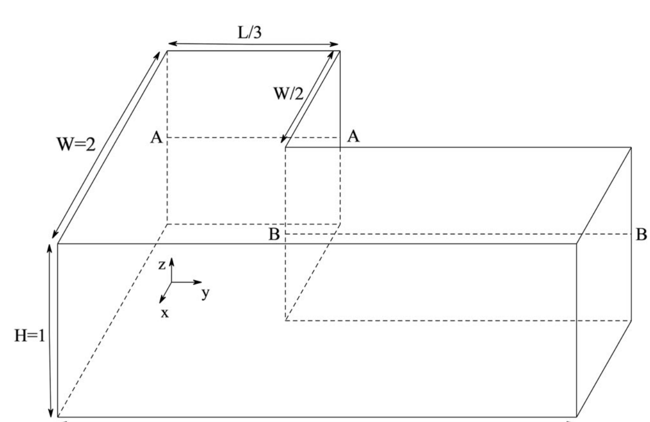

Fig. 3 3D L-shaped geometry and the coordinate origin positioned at the center of the corner diagonal.

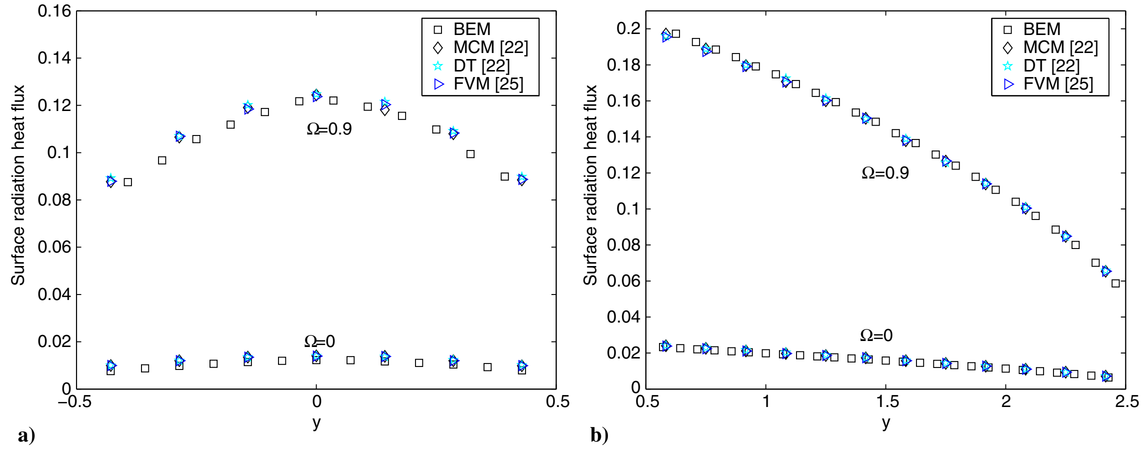

Fig. 4 Surface radiation heat flux at a) the A–A line and b) the B–B line (MCM, Monte Carlo method; DT, discrete transfer method; FVM, finite volume method).

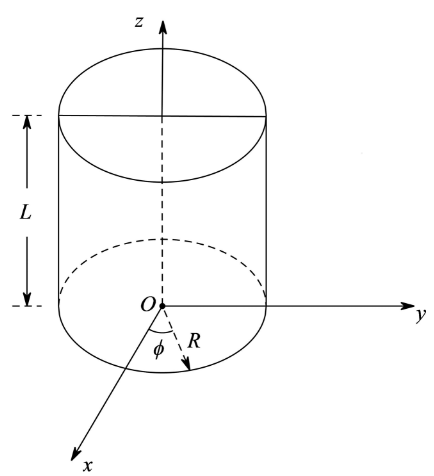

Fig. 5 The cylindrical geometry.

Table 3 Case conditions for continuous property change 3CD solutions

Case	Geometry	Medium property	Surfaces
1	$2R = L = 1$	$\beta = 1, I_b = 1, \Omega = 0.5$	$\epsilon_1 = 1, \epsilon_2 = 1, \epsilon_3 = 0.5(1 - \sin\phi)$
2	$R = L = 1$	$\beta = 1, I_b = 1, \Omega = 1\text{–}0.75r/R$	$\epsilon_1 = 1, \epsilon_2 = 1, \epsilon_3 = 0.5(1 - \sin\phi)$

similar integral form of radiative heat transfer. By these comparisons, the effectiveness and accuracy of our algorithm are further verified.

D. Example 4

In this subsection, the coupled conduction-radiation heat transfer in 3D homogeneous participating media is simulated. The unit cubic geometry is considered again. The bottom surface of the cube is maintained at the high temperature of $T_h = 1000$ K, while the other faces are $T_c = 0.5T_h$. The geometry is shown in Fig. 7. The dimensionless temperature $T^*(= T/T_h)$ along centerline A_1A_2 is presented and compared with the existing results in Fig. 8 [28–30].

From the comparison results in Fig. 8, the present BEM solver is an accurate and reliable numerical technique for the simulation of coupled conduction-radiation heat transfer problems.

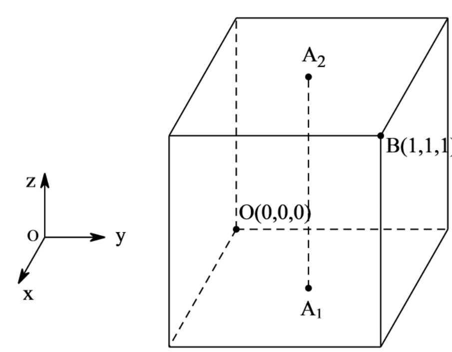

Fig. 7 The unit cube geometry.

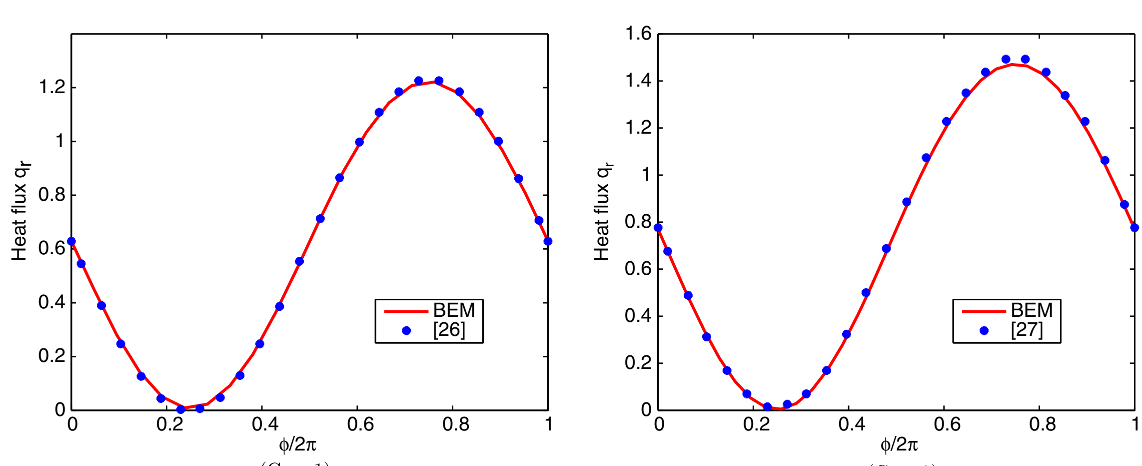

Fig. 6 The distribution of surface radiation heat flux q_r at midplane $z = 0.5L$.

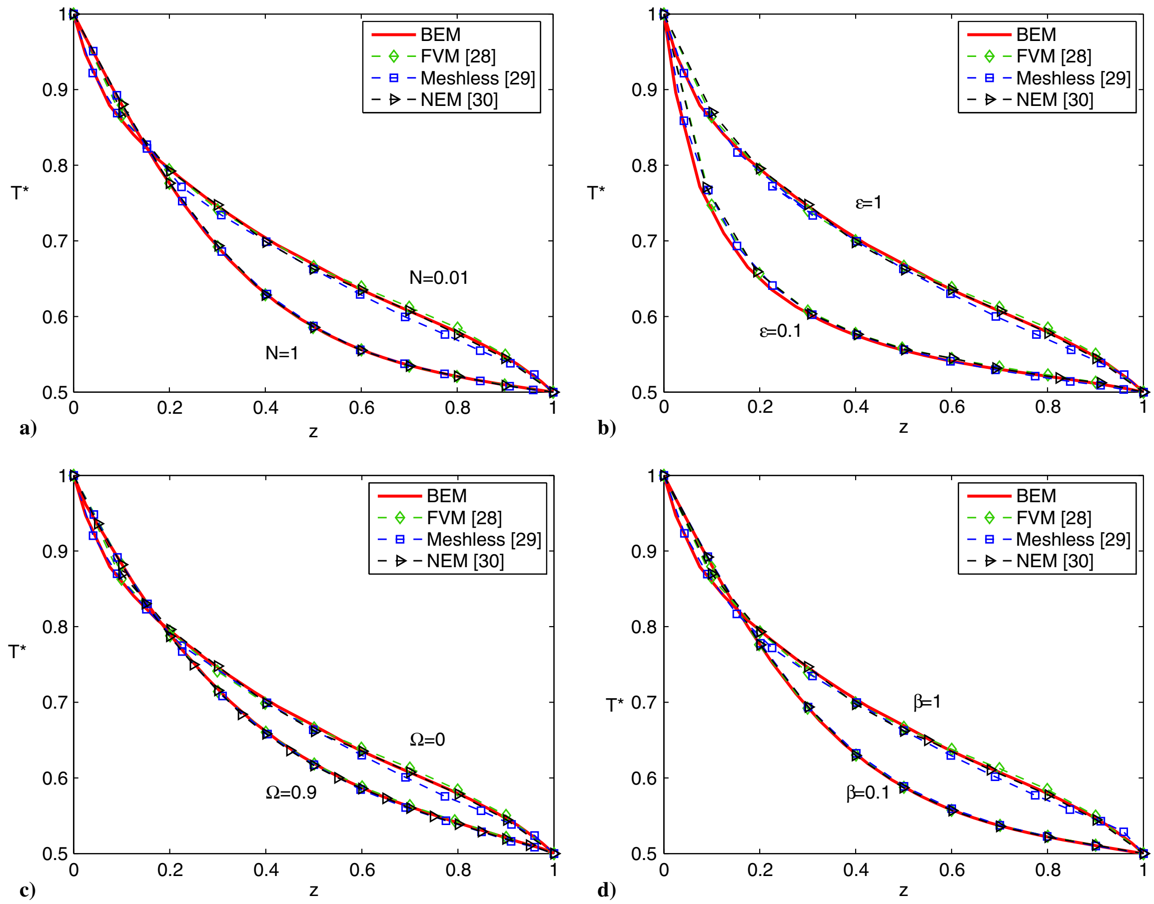

Fig. 8 Effect of various parameters on centerline A_1A_2 temperature along the z direction at $x = 0.5$ and $y = 0.5$ of the cubical enclosure (NEM, natural element method).

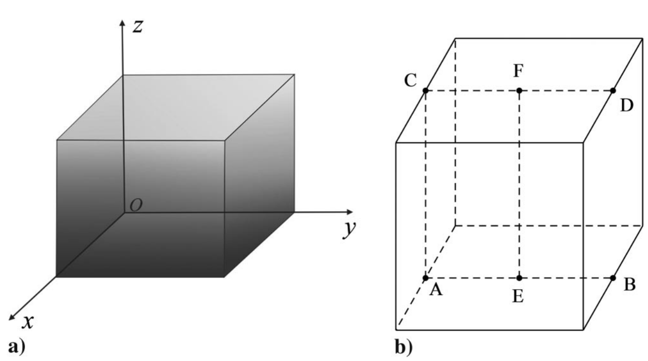

Fig. 9 Geometry illustration: a) the unit cube geometry and b) the illustration of line AB, AC, CD, EF.

E. Example 5

This example is assigned to verify the ability of our present BEM solver for coupled radiation-conduction heat transfer in 3D nonhomogeneous participating media. The problem geometry is shown in Fig. 9a. The bottom boundary is at higher temperature $T_{\mathrm{ref}} = 1000$ K, and all the others are at the same lower temperature $T_c = 500$ K. The emissivity of the boundary is fixed as 0.5. The extinct coefficient and the thermal conductivity vary as

$$\beta(x, y, z) = e^{z \log 9}, \quad k(x, y, z) = 5e^{z \log 9}$$

The dimensionless radiative heat flux $q_r^*(= q_r/(\sigma T_{\mathrm{ref}}^4))$ and dimensionless conduction flux $q_c^*[= q_c/(\sigma T_{\mathrm{ref}}^4)]$ along AB, AC, and CD, as shown in Fig. 9b, are simulated. These data are presented in Table 4. From these results, an obvious fact is that the radiative heat flux increases as the temperature rises.

Additionally, the dimensionless temperature $T^*(= T/T_{\mathrm{ref}})$ along the centerline EF is also calculated. From Fig. 10a, it is found that there are no significant differences between two different grid levels, which are 726 boundary elements and 1350 boundary elements, respectively. This suggests that the BEM solver for the simulation of coupled radiation-conduction heat transfer is accurate and stable. Besides, the cloud map of the resulted temperature field is plotted in Fig. 10b.

Table 4 The dimensionless heat fluxes

AB line			AC line			CD line		
y	q_r^*	q_c^*	z	q_r^*	q_c^*	y	q_r^*	q_c^*
0.1	−0.4026	−0.3346	0.1	0.1325	0.3014	0.1	0.0136	0.0763
0.3	−0.3879	−0.2395	0.3	0.0702	0.1807	0.3	0.0181	0.1321
0.5	−0.3841	−0.2290	0.5	0.0342	0.1397	0.5	0.0197	0.1501
0.7	−0.3879	−0.2395	0.7	0.0160	0.1052	0.7	0.0181	0.1321
0.9	−0.4026	−0.3346	0.9	0.0084	0.0632	0.9	0.0136	0.0763

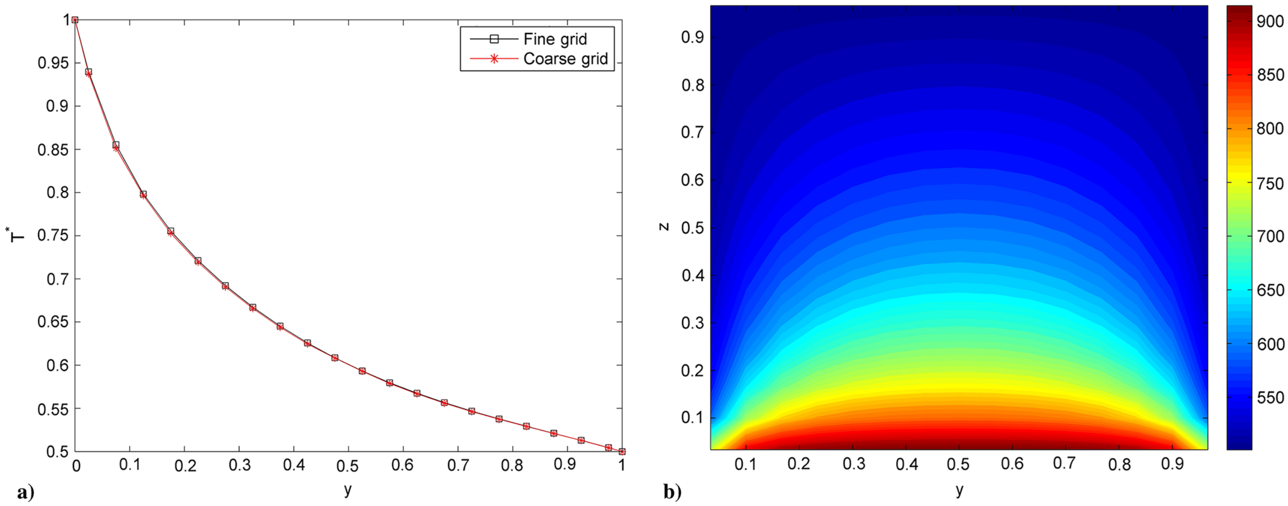

Fig. 10 Temperature distribution: a) the temperature distribution along the centerline EF and b) the temperature field at the plane $x = 0.5$.

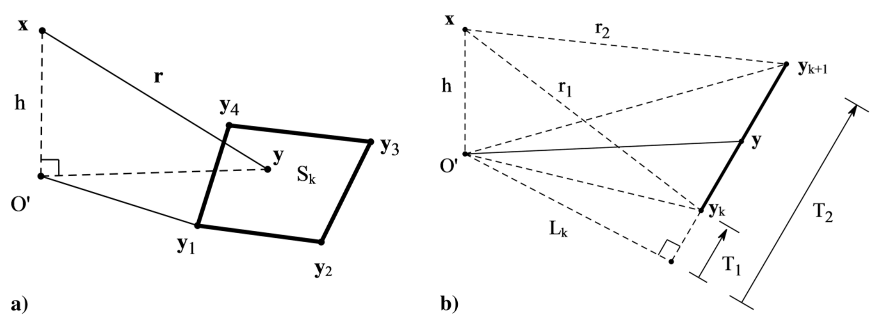

Fig. 11 Analytical integration on an arbitrary quadrilateral element.

IV. Conclusions

The boundary element method (BEM) solver is developed for the predictions of coupled conduction-radiation heat transfer in 3D nonhomogeneous participating media. Three benchmark problems, two belonging to the class of pure radiative heat transfer situation and the third under the class of coupled heat transfer in homogeneous media, were considered to verify the effectiveness of the present algorithm. Then, a 3D coupled conduction-radiation heat transfer in cubic geometry including nonhomogeneous media was simulated by the present BEM solver. For the last example, the numerical results for the percent of radiative heat flux and conduction heat flux and the temperature distribution were given. Although only a kind of situation is simulated, the present algorithm can be applied to arbitrary nonhomogeneous media.

This Paper only considers the solution for the radiative heat transfer in isotropic scattering media. When considering the anisotropic scattering, the formulas (17) and (19) are needed to do some revisions. It is believed that the BEM presented in this Paper can be applied to handle this problem, although there are some improvements in the detailed algorithm. One of the planned future works will be devoted to extending this Paper's algorithm to the anisotropic scattering.

Because of the dense resulting coefficient matrices, the efficient of the BEM has been a serious problem for analyzing large-size models. Fortunately, the fast algorithm, such as the fast multipole method, has been widely introduced in the simulation of the BEM, which makes the computation for large-scale problems possible. So, this is also one of subjects of planned furture research work.

Appendix: Analytical Integration of Kernels in Eq. (41)

The source point $\boldsymbol{x}$ and an arbitrary boundary element S_k are shown in Fig. 11a. The geometry relation between $\boldsymbol{x}$ and one of edge of S_k is shown in Fig. 11b.

First, a local Cartesian coordinate system is introduced. We denote the projection of the source point $\boldsymbol{x}$ onto the plane of the element S_k by O'. Take O' as the origin of the local coordinate system. The basis vector $\boldsymbol{e}_3$ is chosen to be equal to the unit outward normal vector of S_k. The basis vector $\boldsymbol{e}_1$ is an arbitrary unit vector in the plane of S_k. The last basis vector $\boldsymbol{e}_2$ is chosen in such a way that forms the basis $\boldsymbol{e}_1$, $\boldsymbol{e}_2$, $\boldsymbol{e}_3$. Note, too, that the direction of travel on ∂S_k is assumed to be counterclockwise.

The integrations of the three kernels on element S_k can be evaluated analytically as

$$\int_{S_k} G(\boldsymbol{x},\boldsymbol{y})\,\mathrm{d}S(\boldsymbol{y}) = \frac{1}{4\pi}\left\{\sum_{n=1}^{4}\mathrm{sgn}_n\left[L_n \ln\left(\frac{T_2+r_2}{T_1+r_1}\right) + h\arctan\frac{hT_2}{L_n r_2} - h\arctan\frac{hT_1}{L_n r_1}\right] - \alpha'|h|\right\},$$

$$\int_{S_k} \frac{\partial G(\boldsymbol{x},\boldsymbol{y})}{\partial n}\,\mathrm{d}S(\boldsymbol{y}) = -\frac{1}{4\pi}\left\{\sum_{n=1}^{4}\mathrm{sgn}_n\left[\arctan\left(\frac{hT_2}{L_n r_2}\right) - \arctan\left(\frac{hT_1}{L_n r_1}\right)\right] - \mathrm{sign}(h)\alpha'\right\},$$

$$\int_{S_k} \frac{\partial G^*(\boldsymbol{x},\boldsymbol{y})}{\partial n}\,\mathrm{d}S(\boldsymbol{y}) = -\frac{h}{8\pi}\left\{\sum_{n=1}^{4}\mathrm{sgn}_n\left[L_n \ln\left(\frac{T_2+r_2}{T_1+r_1}\right) + h\arctan\frac{hT_2}{L_n r_2} - h\arctan\frac{hT_1}{L_n r_1}\right] - \alpha'|h|\right\}$$

where

$$\mathrm{sgn}_i = \mathrm{sign}[(\boldsymbol{y}_k - O')\cdot \boldsymbol{n}_i],$$

$$\alpha' = \begin{cases} 0, & O' \notin \bar{S}_k, \\ \alpha, & O' \in \bar{S}_k \end{cases}$$

α is the internal angle with regard to $\boldsymbol{y}$ on the element, and $\boldsymbol{n}_i$ denotes the outward normal vector of ith edge of the element.

Acknowledgments

This research was financially supported by the National Natural Science Foundation of China (grant numbers 11471262 and 11401208).

References

[1] Li, H. Y., Ozisik, M. N., and Tsai, J. R., "Two-Dimensional Radiation in a Cylinder with Spatially Varying Albedo," *Journal of Thermophysics and Heat Transfer*, Vol. 6, No. 1, 1992, pp. 180–182. doi:10.2514/3.340

[2] Bialecki, R. A., *Solving Heat Radiation Problems Using the Boundary Element Method*, Computational Mechanics, Southampton, England, U. K., 1993, pp. 1–137.

[3] Blobner, J., Bialecki, R. A., and Kuhn, G., "Transient Non-Linear Heat Conduction: Radiation Problems, a Boundary Element Formulation," *International Journal for Numerical Methods in Engineering*, Vol. 46, No. 11, 1999, pp. 1865–1882. doi:10.1002/(ISSN)1097-0207

[4] Blobner, J., Bialecki, R. A., and Kuhn, G., "Boundary-Element Solution of Coupled Heat Conduction-Radiation Problems in the Presence of Shadow Zones," *Numerical Heat Transfer, Part B: Fundamentals*, Vol. 39, No. 5, 2001, pp. 451–478. doi:10.1080/104077901750188840

[5] Qatanani, N., and Schulz, M., "Analytical and Numerical Investigation of the Fredholm Integral Equation for the Heat Radiation Problem," *Applied Mathematics and Computation*, Vol. 175, No. 1, 2006, pp. 149–170. doi:10.1016/j.amc.2005.07.017

[6] Sun, B., Zheng, D., Klimpke, B., and Yildir, B., "Modified Boundary Element Method for Radiative Heat Transfer Analyses in Emitting, Absorbing and Scattering Media," *Engineering Analysis with Boundary Elements*, Vol. 21, No. 2, 1998, pp. 93–104. doi:10.1016/S0955-7997(97)00068-4

[7] Li, B. Q., Cui, X., and Song, S. P., "The Galerkin Boundary Element Solution for Thermal Radiation Problems," *Engineering Analysis with Boundary Elements*, Vol. 28, No. 7, 2004, pp. 881–892. doi:10.1016/j.enganabound.2004.01.009

[8] Clements, D. L., "A Boundary Integral Equation Method for the Numerical Solution of a Second Order Elliptic Equation with Variable Coefficients," *ANZIAM Journal*, Vol. 22, No. 2, 1980, pp. 218–228.

[9] Gray, L. J., Kaplan, T., Richardson, J. D., and Paulino, G. H., "Green's Functions and Boundary Integral Analysis for Exponentially Graded Materials: Heat Conduction," *Journal of Applied Mechanics*, Vol. 70, No. 4, 2003, pp. 543–549. doi:10.1115/1.1485753

[10] Kassab, A. J., and Divo, E., "A Generalized Boundary Integral Equation for Isotropic Heat Conduction with Spatially Varying Thermal Conductivity," *Engineering Analysis with Boundary Elements*, Vol. 18, No. 4, 1996, pp. 273–286. doi:10.1016/S0955-7997(96)00057-4

[11] Power, H., "On the Existence of Kassab and Divo's Generalized Boundary Integral Equation Formulation for Isotropic Heterogeneous Steady State Heat Conduction Problems," *Engineering Analysis with Boundary Elements*, Vol. 20, No. 4, 1997, pp. 341–345. doi:10.1016/S0955-7997(97)00114-8

[12] Bonnet, M., and Guiggiani, M., "Comments about the Paper Entitled 'A Generalized Boundary Integral Equation for Isotropic Heat Conduction with Spatially Varying Thermal Conductivity," edited by A. J. Kassab, and E. Divo, *Engineering Analysis with Boundary Elements*, Vol. 22, No. 3, Elsevier, 1998, pp. 235–240. doi:10.1016/S0955-7997(98)00046-0

[13] Berger, J. R., Martin, P. A., Mantic, V., and Gray, L. J., "Fundamental Solutions for Steady-State Heat Transfer in an Exponentially Graded Anisotropic Material," *Zeitschrift für angewandte Mathematik und Physik ZAMP*, Vol. 56, No. 2, 2005, pp. 293–303. doi:10.1007/s00033-004-1131-6

[14] Mikhailov, S. E., "Localized Boundary-Domain Integral Formulations for Problems with Variable Coefficients," *Engineering Analysis with Boundary Elements*, Vol. 26, No. 8, 2002, pp. 681–690. doi:10.1016/S0955-7997(02)00030-9

[15] Al-Jawary, M. A., and Wrobel, L. C., "Radial Integration Boundary Integral and Integro-Differential Equation Methods for Two-Dimensional Heat Conduction Problems with Variable Coefficients," *Engineering Analysis with Boundary Elements*, Vol. 36, No. 5, 2012, pp. 685–695. doi:10.1016/j.enganabound.2011.11.019

[16] Sutradhar, A., and Paulino, G. H., "A Simple Boundary Element Method for Problems of Potential in Non-Homogeneous Media," *International Journal for Numerical Methods in Engineering*, Vol. 60, No. 13, 2004, pp. 2203–2230. doi:10.1002/(ISSN)1097-0207

[17] Gao, X. W., "A Meshless BEM for Isotropic Heat Conduction Problems with Heat Generation and Spatially Varying Conductivity," *International Journal for Numerical Methods in Engineering*, Vol. 66, No. 9, 2006, pp. 1411–1431. doi:10.1002/(ISSN)1097-0207

[18] Yang, K., Wang, J., Du, J. M., Peng, H. F., and Gao, X. W., "Radial Integration Boundary Element Method for Nonlinear Heat Conduction Problems with Temperature-Dependent Conductivity," *International Journal of Heat and Mass Transfer*, Vol. 104, No. 1, 2017, pp. 1145–1151. doi:10.1016/j.ijheatmasstransfer.2016.09.015

[19] Modest, M. F., *Radiative Heat Transfer*, Academic Press, New York, 2013, pp. 295–296.

[20] Viskanta, R., "Radiation Transfer and Interaction of Convection with Radiation Heat Transfer," *Advances in Heat Transfer*, Vol. 3, No. 1, 1996, pp. 176–251.

[21] Han, Y., and Nie, Y., "Analytical and Numerical Investigation of Radiative Heat Transfer in Semitransparent Media," arXiv:1709.04769, 2017, arxiv.org/abs/1709.04769.

[22] Henson, J. C., and Malalasekera, W. M. G., "Comparison of the Discrete Transfer and Monte Carlo Methods for Radiative Heat Transfer in Three-Dimensional Nonhomogeneous Scattering Media," *Numerical Heat Transfer*, Vol. 32, No. 1, 1997, pp. 19–36. doi:10.1080/10407789708913877

[23] Hsu, P. F., and Farmer, J. T., "Benchmark Solutions of Radiative Heat Transfer Within Nonhomogeneous Participating Media Using the Monte Carlo and YIX Method," *Journal of Heat Transfer*, Vol. 119, No. 1, 1997, pp. 185–188. doi:10.1115/1.2824087

[24] Burns, S. P., Howell, J. R., and Klein, D. E., "Finite Element Solution for Radiative Heat Transfer with Nongray, Nonhomogeneous Radiative Properties," *Proceedings of the 30th National Heat Transfer Conference*, Vol. 13, American Soc. of Mechanical Engineers, Portland, OR, 1995, pp. 3–10.

[25] Kamel, G., Naceur, B. M., Rachid, M., and Rachid, S., "Formulation and Testing of the FTn Finite Volume Method for Radiation in 3-D Complex Inhomogeneous Participating Media," *Journal of Quantitative Spectroscopy and Radiative Transfer*, Vol. 98, No. 3, 2006, pp. 425–445. doi:10.1016/j.jqsrt.2005.07.001

[26] Chen, X. L., and Sutton, W., "Radiative Transfer in Finite Cylindrical Media Using Transformed Integral Equations," *Journal of Quantitative Spectroscopy and Radiative Transfer*, Vol. 77, No. 3, 2003, pp. 233–271. doi:10.1016/S0022-4073(02)00124-3

[27] Sutton, W. H., and Chen, X. L., "A General Integration Method for Radiative Transfer in 3-D Non-Homogeneous Cylindrical Media with Anisotropic Scattering," *Journal of Quantitative Spectroscopy and Radiative Transfer*, Vol. 84, No. 1, 2004, pp. 65–103. doi:10.1016/S0022-4073(03)00117-1

[28] Talukdar, P., Issendorff, F. V., Trimis, D., and Simonson, C. J., "Conduction-Radiation Interaction in 3D Irregular Enclosures Using the Finite Volume Method," *Heat and Mass Transfer*, Vol. 44, No. 6, 2008, pp. 695–704. doi:10.1007/s00231-007-0303-2

[29] Sadat, H., Wang, C. A., and Le Dez, V., "Meshless Method for Solving Coupled Radiative and Conductive Heat Transfer in Complex Multi-Dimensional Geometries," *Applied Mathematics and Computation*, Vol. 218, No. 20, 2012, pp. 10211–10225. doi:10.1016/j.amc.2012.03.101

[30] Zhang, Y., Ma, Y., Yi, H. L., and Tan, H. P., "Natural Element Method for Solving Radiative Transfer with or Without Conduction in Three-Dimensional Complex Geometries," *Journal of Quantitative Spectroscopy and Radiative Transfer*, Vol. 129, No. 1, 2013, pp. 118–130. doi:10.1016/j.jqsrt.2013.06.002